Atmos. Chem. Phys. Discuss., 11, 17423–17445, 2011
www.atmos-chem-phys-discuss.net/11/17423/2011/
doi:10.5194/acpd-11-17423-2011

Atmospheric Chemistry and Physics Discussions

Theory of isotope fractionation on facetted ice crystals

J. Nelson

Laucks Foundation Inc. Suite 2100, PMB 174, 1700 Seventh Ave., Seattle WA 98101, USA

Received: 8 May 2011 – Accepted: 6 June 2011 – Published: 21 June 2011

Correspondence to: J. Nelson (jontne@gmail.com)

Published by Copernicus Publications on behalf of the European Geosciences Union.

Abstract

Present models of the differential incorporation of isotopic water molecules into vapor-grown ice omit surface processes that may be important in temperature reconstructions. This article introduces a model that includes such surface processes and shows that differences in deposition coefficients for water isotopes can produce isotope fractionation coefficients that significantly differ from those of existing theory. For example, if the deposition coefficient of $H_2^{18}O$ differs by just 5 % from that of ordinary water ($H_2^{16}O$), the resulting fractionation coefficient at 20 % supersaturation may deviate from the kinetic fractionation (KF) prediction by up to about ±17 ‰. Like the KF model, this "surface-kinetic" fractionation model generally predicts greater deviation from the equilibrium prediction at higher supersaturations; indeed, the sensitivity to supersaturation far exceeds that to temperature. Moreover, the model introduces possible new temperature dependencies from the deposition coefficients. These parameters need to be constrained by new laboratory measurements; nevertheless, the theory suggests that observed $\delta^{18}O$ changes in ice samples are unlikely to be due solely to temperature changes.

1 Introduction

Ever since the late 1950s, the fractionation of isotopes during the vapor deposition of ice has been used to infer trends in the crystal's formation temperature (see, e.g., Langway Jr., 2008). For example, the empirical relation between $\delta^{18}O$ in surface snow and the mean surface temperature of a given region has been used to estimate trends in the formation temperatures of ancient ice from ice cores of the same region (e.g., Dansgaard et al., 1969). However, because crystals form at various regions of the atmosphere and grow while falling through layers of variable temperature, the mean surface temperature does not equal the crystal condensation temperature. So, how precisely can we determine a crystal's condensation temperature based on its isotope content?

ACPD
11, 17423–17445, 2011

Equilibrium fractionation theory has been used to infer crystal condensation temperatures. But in 1984, Jouzel and Merlivat, hereafter "JM", showed that this theory disagrees with the empirical surface-snow relation. Their solution was to replace the equilibrium fractionation coefficient with a supersaturation-dependent kinetic fractionation (KF) coefficient. By selecting the right supersaturation-temperature relation, their model could fit the δ^{18}O observations. But the KF coefficient ignores surface processes that are crucial to the growth of facetted crystals. If we consider such processes in a new theory, how much might the fractionation coefficient change? And could this change affect temperature reconstructions?

This paper develops a theory of fractionation on facetted crystals that includes surface processes. The resulting fractionation coefficient α differs from the KF prediction by an amount $\Delta\alpha$ that may be as large as ±17‰. As described in Sect. 5, this $\Delta\alpha$ gives an uncertainty in the inferred (i.e., reconstructed) temperature of 15 °C, though in practice, various factors will lower the uncertainty. But because the surface effect is potentially large, new experiments on α for facetted crystals are greatly needed.

2 Background

2.1 Facetted growth implies regulation by surface processes

The surface of growing atmospheric ice crystals often consists of crystalline facets, sometimes wholly so, which indicates a reduction of growth rate from surface processes (Nelson and Baker, 1996). Without such surface processes, an initially spherical frozen droplet would remain spherical as the crystal grew until being perturbed by a sufficiently large temperature or vapor-density non-uniformity, after which rounded protrusions would develop. Instead, initially spherical frozen droplets quickly grow into a great variety of shapes. Thus, the existence of facets, however small, indicate an influence of surface processes, and if these processes affect the incorporation of ordinary water into ice, they are likely to also affect the incorporation of isotopic water. That is, surface processes should affect isotope fractionation.

ACPD
11, 17423–17445, 2011

2.2 Crystal growth with vapor and surface impedances

The net vapor flux F ($\#\,m^{-2}\,s^{-1}$) of ordinary water molecules to an ice surface is (e.g., Nelson and Baker, 1996)

$$F = \frac{v}{4}\beta(N_S - N_{EQ}) \equiv \frac{v}{4}\beta N_{EQ}\sigma_S, \quad (1)$$

where v is the mean vapor-molecule speed, N_S is the vapor number density at the surface ($\#\,m^{-3}$), N_{EQ} is the equilibrium vapor number density, a function of the surface temperature T_S, σ_S is the surface supersaturation, and β is the deposition coefficient function. In general, β ranges between 0 and 1, depending on both T_S and σ_S, and depends on whether the crystal face is basal, prism, or some other orientation. Through Sect. 3, we assume all faces are identical and thus described by just one β. In Sect. 4, we consider more realistic crystals with two face types. Symbols used throughout the text are tabulated in Appendix D.

The surface supersaturation lies below the far-field supersaturation $\sigma_\infty \equiv (N_\infty - N_{EQ})/N_{EQ}$, where N_∞ is the far-field vapor density, by an amount that depends on how the surface and surroundings impede growth. Specifically,

$$\sigma_S = \frac{\sigma_\infty}{\beta Z}, \quad (2)$$

where Z, a dimensionless number, is the total impedance to growth discussed below (Kuroda, 1984; Yokoyama and Kuroda, 1990; Nelson and Baker, 1996). Here and elsewhere, the same relations also hold for each isotope type, whether HDO (i.e., $HD^{16}O$) or $H_2^{18}O$, except with different values of the quantities F, v, N_S, N_{EQ}, β, N_∞, and Z. These quantities thus have superscript "i", which stands for either "HDO" or "$H_2^{18}O$".

The total impedance equals the sum of Z_V, the vapor diffusion impedance, Z_H, the thermal impedance, and Z_S, the surface impedance. Z_V accounts for the impedance of the vapor diffusing through air to the crystal surface and increases in proportion to

ACPD
11, 17423–17445, 2011

the crystal size (Appendix A). Larger crystals are surrounded by larger vapor-depleted regions and thus have greater impedance. As an example, at sea-level pressure, a spherical crystal starting at 1-μm radius and ending at 500 μm has Z_V values increasing from 7.5 to 3700. At lower pressures, Z_V decreases in proportion to the pressure decrease. The thermal impedance arises from the temperature rise of the crystal, the temperature at which the latent heating balances thermal diffusion to the surrounding air. Its magnitude decreases rapidly with decreasing temperature (in proportion to N_{EQ}) and is less than Z_V below about −5 °C (Nelson and Baker, 1996). So to simplify the expressions, we drop Z_H, though it can easily be added to Z_V in all that follows.

The surface impedance equals the inverse of the deposition coefficient:

$$Z_S \equiv \frac{1}{\beta}. \tag{3}$$

This impedance results from an increase in surface-mobile molecules that desorb from the surface. The number of such molecules per area of surface exceeds the equilibrium value because the supersaturated vapor produces a greater-than-equilibrium flux of molecules to the surface and some of the excess molecules do not reach the strong-binding sites on a surface step. Thus, a molecule may fail to reach a step, or having reached a step, fail to bind to the step. On a micron-or-larger facet, the fraction of the incident molecules that reach a step should be significantly below unity.

3 Basic theory of surface-kinetic fractionation

Under constant conditions, the ratio χ of the number of isotope molecules to H_2O molecules in the crystal equals the ratio of their respective net vapor fluxes to the surface. From Eqs. (1) and (2), this ratio equals

ACPD
11, 17423–17445, 2011

$$\chi = \frac{(N^i_\infty - N^i_{\mathrm{EQ}})}{N_{\mathrm{EQ}}\sigma_\infty d'} \frac{1+z}{1+z^i}, \tag{4}$$

where $z \equiv Z_S/Z_V$, the ratio of surface impedance to that of vapor diffusion, and $d' \equiv D/D^i$, the ratio of the vapor diffusion constants. But, by definition of the equilibrium fractionation coefficient α_S (JM, Eq. 7), the corresponding isotopic number ratio in the vapor differs from that in the solid by the equilibrium fractionation ratio for ice:

$$\frac{N^i_{\mathrm{EQ}}}{N_{\mathrm{EQ}}} = \frac{\chi}{\alpha_S}. \tag{5}$$

(Formulas in Jouzel, 1986 for α_S are $\ln\alpha_S = 11.839/T - 28.224\times10^{-3}$ for $H_2^{18}O$ and $\ln\alpha_S = 16288/T^2 - 9.34\times10^{-2}$ for HDO.) We define the nonequilibrium fractionation coefficient α like that in Eq. (5) except with the far-field, non-equilibrium, vapor density:

$$\frac{N^i_\infty}{N_\infty} = \frac{\chi}{\alpha}. \tag{6}$$

Using Eqs. (4), (5), and (6) to eliminate N^i_{EQ},N^i_∞, and χ, one gets

$$\alpha = \frac{1+\sigma_\infty}{\frac{1}{\alpha_S} + \sigma_\infty d' \frac{1+z^i}{1+z}}. \tag{7}$$

Three limits of Eq. (7) stand out: the equililbrium limit, the KF limit, and the surface-kinetic limit. In the first, $\alpha \to \alpha_S$ when $\sigma_\infty \to 0$. In the KF limit, the surface impedances vanish ($z, z^i \to 0$) giving

ACPD
11, 17423–17445, 2011

$$\alpha_{KF} = \frac{1 + \sigma_\infty}{\frac{1}{\alpha_S} + \sigma_\infty d'}, \quad (8)$$

which shows that KF fractionation occurs whenever $d' \neq 1/\alpha_S$. Equation (8) agrees with JM's result, though they wrote the equivalent expression as $\alpha_K \cdot \alpha_S$. (Fisher, 1991 does a more detailed analysis of the temperature difference between crystal and air, but the result is nearly indistinguishable from the KF result.) Finally, in the surface-kinetic limit ($z, z^i \gg 1$)

$$\alpha_{SK} = \frac{1 + \sigma_\infty}{\frac{1}{\alpha_S} + \sigma_\infty y x}, \quad (9)$$

where $y \equiv v/v^i$ and $x \equiv \beta/\beta^i$. Equation (9) shows that surface fractionation occurs when $y \cdot x \neq 1/\alpha_S$.

Thus, fractionation depends on four factors: α_S, d', y, and x. Physically, α_S arises from different isotopic rates of desorption of an equilibrium distribution of water species on the ice surface. But under supersaturated conditions, vapor flows to the ice surface, producing additional fractionation due to different isotopic rates of vapor diffusion (d'), molecular impingement to the surface (y), and desorption from the surface (x). The isotopic desorption rates change because the surface has a greater-than-equilibrium concentration of mobile water species; the species with a lower deposition coefficient will have a greater increase in mobile molecules on the surface, and thus a corresponding increase in desorption rate. The first three factors are close to unity (Table 1) and independent of supersaturation. However, x may vary with supersaturation and is presently unknown. Here, we assume a range of $0.8 \leq x \leq 1.2$ as described in Appendix B.

For surface fractionation to be significant, z must be non-negligible, meaning the surface impedance must be large. To determine the surface impedance, we must

ACPD
11, 17423–17445, 2011

estimate β and β^i for a given set of conditions. These conditions influence β because β depends on σ_S. We can approximate a range of cases using two parameters σ_1 and n as

$$\beta = (\frac{\sigma_S}{\sigma_1})^n, \quad (10)$$

where $n > 0$ and σ_1 is a characteristic supersaturation that depends on temperature and surface properties of the crystal facet. To determine β and σ_S, one must combine Eq. (10) with Eqs. (2) and (3). In the linear and quadratic cases ($n = 1$ or 2), one can solve for β analytically and deduce σ_S, but the general case requires a numerical method. Numerical results are described in Appendix C and used in the calculations for Figs. 1 and 2.

At a given temperature and supersaturation, two variable factors affect α: the surface impedance ratio z for regular water and the ratio of surface impedances x. The former increases with an increase in either the parameter σ_1 or n, but decreases with increasing crystal size, as shown in Fig. 1. In addition, z increases with elevation due to the air-pressure dependence of the vapor diffusion constant.

Deviations from the KF prediction occur at large z and when x differs from the KF limit of d'. When $x < 1$, the deposition coefficient of the isotope exceeds that of regular water, making the ice richer in isotope by an amount that depends on z. For example, at relatively high surface impedance, as in the upper "beaded" curve in Fig. 2 ($z > 3$ over the entire supersaturation range), the fractionation lies above the KF value because $x = 0.95$, which is less than $d' = 1.03$. But, as x is not below $1/\alpha_S$, the fractionation does not exceed the equilibrium value, instead lying roughly halfway between the KF and equilibrium values. Similarly, when $x > d'$, the surface fractionation acts in the same direction as KF, driving the degree of fractionation even lower. For example, when x is instead 1.05, the fractionation lies distinctly below the KF curve (Fig. 2, lower beaded curve). In this case, the fractionation from y acts together with that from x, increasing the effect.

ACPD
11, 17423–17445, 2011

If x deviates further from unity, the surface impedance need not be large for surface fractionation to have a large effect. For example, with middling values of z, the fractionation exceeds α_S when $x = 0.8$ (Fig. 2, top curve). And when $x = 1.2$, the surface fractionation may lie below the KF value by an amount nearly double the amount KF lies below the equilibrium value (Fig. 2, bottom curve). In contrast, at low surface impedance, the fractionation remains close to the KF value even when the x value deviates 20 % from unity.

4 Surface-kinetic fractionation to realistic crystals

4.1 Cylindrical crystals

We now make the model more realistic by considering crystals shaped as tabular or columnar cylinders. In addition to introducing the variable length/diameter ratio, the cylinder case has two distinct faces, with the top/bottom, or "basal" face having fractionation value α_B, and the side or "prism" face having value α_P.

These fractionation values follow from Eq. (7) with the appropriate substitution; for example, for α_B, we substitute z_B for z and z_B^i for z^i. Concerning z_B and z_P, the surface impedances equal the reciprocals of β_B and β_P, just as in the sphere case, but the vapor impedances are more complex, depending not only on crystal size, but also on shape and rate of shape change (see Appendix A).

To determine values for $\alpha_{B,P}$, one must know the deposition coefficients, which means determining just one number: σ_S. With a nonspherical crystal such as the cylinder, σ_S varies along the surface. But, as described elsewhere (e.g., Wood et al., 2001), the point of highest σ_S determines the growth rate and thus is the appropriate σ_S value for the deposition coefficient (Eq. 10). This point is usually the edge of the facet (unless some face has essentially stopped growing; Nelson, 2001). Here, we assume

ACPD
11, 17423–17445, 2011

this is the case for both the basal and prism facets. As a result, the σ_S value solves

$$\sigma_S = \frac{\sigma_\infty}{1+\beta_B(\sigma_S)Z_{VB}} = \frac{\sigma_\infty}{1+\beta_P(\sigma_S)Z_{VP}}, \quad (11)$$

which is similar to Eq. (2).

To get the mass-averaged α_s one multiplies each coefficient by the mass-uptake (flux times facet area) on the corresponding facets:

$$\alpha = \alpha_B \frac{\gamma}{\gamma+2\Gamma} + \alpha_P \frac{2\Gamma}{\gamma+2\Gamma}, \quad (12)$$

where $\gamma \equiv \beta_B/\beta_P$ is the growth-rate ratio (Nelson and Baker, 1997) and Γ is the length-diameter ratio (aspect ratio). For example, in steady-state, $\gamma = \Gamma$, and thus 2/3 of the mass enters via the prism faces. But in general, a range of fractionation values can occur, depending on the crystal aspect ratio, the growth-rate ratio, and the fractionation to each face. The last factor depends on the ratios of the deposition coefficient functions $x_B \equiv \beta_B/\beta_B^i$ and $x_P \equiv \beta_P/\beta_P^i$.

Results show that the crystal shape affects fractionation at high z, particularly when the deposition coefficient ratios differ between the faces. For example, when $z > 2.5$ (all solid curves in Fig. 3), but both facets have the same x ratio of 1.05, the fractionation coefficient is only slightly less than the sphere result. This is shown by curve 1 in which $\Gamma = \gamma = 10$. At larger Γ, the fractionation coefficient decreases further, though the effect remains relatively small. Larger influences on α can occur when $x_B \neq x_P$. In particular, for steady-state growth ($\gamma = \Gamma$ with $\Gamma = 10$, fractionation decreases when $x_P > x_B$ (curve 2), even though their average still equals 1.05 because in steady state most mass enters through the prism face, which has an x_P value of 1.1.

Usually Γ deviates further and further from unity during growth (Takahashi et al., 1991), meaning $\gamma \geq \Gamma$ for columns and $\gamma \leq \Gamma$ for plates. In the non-steady-state case of curve 3, most mass enters through the basal face, and in this case $x_B = 1.1$, bringing the curve lower. Similarly, when nearly all of the mass enters through the prism face,

ACPD
11, 17423–17445, 2011

as in the tabular-crystal case in curve 4, then the fractionation coefficient is significantly below that of the sphere when $x_P = 1.1$. These cases (2–4) show deviations in α below that of an equivalent sphere of $x = 1.05$ because the face with most of the mass uptake had $x = 1.10$. If instead they had $x = 1.00$, then the resulting α value would be above that of a sphere. These cylinder results emphasize what we found with the sphere: when the surface impedance dominates, small changes in x can introduce relatively large variations in fractionation coefficient. For the cylinder, this applies to small changes in x on the facets that dominate growth.

4.2 Incompletely facetted crystals

Stellar and hollowed crystals are incompletely facetted, meaning that some of the mass uptake comes from non-facetted (NF) regions. For this case, we need an extra term in Eq. (12):

$$\alpha = \alpha_B M_B + \alpha_P M_P + \alpha_{NF} M_{NF}, \quad (13)$$

where M_j stands for the fraction of mass uptake that occurs through face type "j" and α_{NF} equals the fractionation coefficient for non-facetted regions. The latter coefficient should equal α with $\beta \to 1$, and thus nearly equal α_{KF}.

For stellar or dendritic crystals, it is hard to accurately estimate M_P and M_{NF} without newer, more careful measurements. I attempted such an estimate in Nelson (2005), using the measurements of Takahashi et al. (1991), and found that M_{NF} varied between 0.77 and 0.87 for crystals between −13.3 and −16.8 °C. Thus, most of the mass uptake on such crystals occurs on the non-facet regions.

A similar difficulty occurs with hollowed columns, except the problem instead lies in estimating M_B and M_{NF}. However, if we assume that the hollowed regions are cylindrical cones extending to the crystal center, and if the volume of the hollows remain a fixed fraction K of the volume of the equivalent non-hollowed crystal, then the resulting

ACPD
11, 17423–17445, 2011

mass-uptake fractions can be shown to equal

$$M_{\mathrm{B}} = \frac{\gamma}{\gamma + 2\Gamma}\frac{1-3K}{1-K}, \cdot M_{\mathrm{P}} = \frac{2\Gamma}{\gamma + 2\Gamma}\frac{1}{1-K}, \cdot M_{\mathrm{NF}} = \frac{2K}{\gamma + 2\Gamma}\frac{\gamma - \Gamma}{1-K}. \quad (14)$$

When the hollow extends across the entire basal face, K has its maximum value of 1/3. In this case, $M_{\mathrm{B}} = 0$ and the fraction of mass uptake by the non-facet region M_{NF} has its maximum value, a value that depends on γ/Γ. Using the measurements for hollow columns at −5.3 °C from Takahashi et al. (1991), $\gamma/\Gamma = 5.4$, giving $M_{\mathrm{NF}} = 0.6$. As the hollows did not appear to extend across the basal faces, this value may be an overestimate. Nevertheless, significant amounts of uptake likely occur in the non-facet regions of hollow columns.

5 Discussion: the need for new measurements

In many regions, precipitating ice largely consists of single-crystalline and aggregates of incompletely facetted forms, forms for which the existing KF model may suffice because of the large uptake on non-facetted regions. However, precipitating crystals in polar regions (e.g., Lawson et al., 2006), crystals in cirrus and other high clouds, as well as surface hoar often consist of mainly facetted forms for which the new surface-kinetic model may be required.

To estimate how the present uncertainty in α for facetted crystals could produce uncertainty in inferred temperature T' of precipitated ice, we transform the uncertainty in α to the uncertainty in the relative deviation of isotopic content in ice δ_{C}, and then this uncertainty to a temperature uncertainty. In our notation

$$\delta_{\mathrm{C}} = \frac{\chi - \chi_{\mathrm{SMOW}}}{\chi_{\mathrm{SMOW}}} = \alpha\frac{N_{\infty}^{i}/N_{\infty}}{\chi_{\mathrm{SMOW}}} - 1, \quad (15)$$

ACPD
11, 17423–17445, 2011

and thus an uncertainty in α of $\Delta\alpha$ gives an uncertainty in δ_C of

$$\Delta\delta_C = \Delta\alpha \frac{N^i_\infty / N_\infty}{\chi_{SMOW}} \approx \Delta\alpha. \quad (16)$$

Using the modeled gradient of ^{18}O with respect to the condensation temperature $d\delta_C^{18}O/dT_C$ from Jouzel et al. (1997), the uncertainty in inferred temperature T' of precipitated ice is approximately

$$\Delta T' \approx \frac{\Delta\delta_C}{d\delta_C{}^{18}O/dT_C} \approx \frac{\Delta\alpha}{1.1}. \quad (17)$$

Thus, equating the possible range in α from Fig. 2 ($\sim \pm 17$ ‰) to the uncertainty $\Delta\alpha$ the uncertainty in the inferred crystal growth temperature equals about 15 °C, a large value. However, the uncertainty in the inferred paleoclimatic condensation temperatures would probably be much less, reflecting a convolution of $\Delta\alpha$ with the relative changes in supersaturation and degree of crystal faceting during a past climate shift. The effect of surface-kinetic fractionation may also be lessened because the ice record in a given layer is the yearly accumulation, and thus will have a greater mass contribution per crystal from the larger crystals that have less uptake on facets.

Nevertheless, the surface effect, large or small is unknown. Previous vapor-to-ice fractionation experiments are limited to largely non-facetted crystals. Specifically, Jouzel and Merlivat (1984) exposed a −20 °C surface to water vapor at 20 °C, conditions that produce highly dendritic frost crystal forms. Uemura et al. (2005) analyzed similarly dendritic frost forms. Thus, although those experiments were appropriate for testing the KF model, they cannot be used to understand surface fractionation. Instead, to test this model, we need new experiments on completely facetted crystals.

Moreover, because α depends on both T and σ_∞, if we measure the dependence for both HDO and $H_2^{18}O$, one could then, in principle, use observed $\delta^{18}O$ and δ_D values to infer both the deposition temperature and supersaturation of an ice sample.

ACPD
11, 17423–17445, 2011

6 Conclusions

Unlike kinetic fractionation theory, the surface-kinetic theory includes potentially important surface processes on facetted ice crystals. When the surface impedance to growth is low, both the kinetic and surface-kinetic models give similar predictions, showing significant deviations to equilibrium fractionation at moderate-to-high supersaturations. In contrast, when the surface impedance is comparable to the vapor impedance, the fractionation coefficient depends sensitively on the ratio of the deposition coefficient functions of the ordinary and isotopic water molecules, giving results that deviate sharply from kinetic fractionation results. Such conditions should hold during the growth of facetted crystals, and since facetted crystals are common in the atmosphere, the new theory should apply to some cases in which the kinetic and the equilibrium theory have previously been used. However, before the new theory can be applied to the atmosphere, we need to either measure the effect directly or experimentally determine the relevant deposition coefficient functions over a range of temperatures and supersaturations.

Appendix A

The vapor impedances

The vapor impedance depends on the crystal shape. For a spherical crystal

$$Z_{\mathrm{V}} \equiv \frac{rv}{4D}, \tag{A1}$$

where r is the radius of the crystal and D is the vapor diffusion constant. For a cylindrical crystal

ACPD
11, 17423–17445, 2011

$$Z_{VB} = r_B h_{BE} + r_P h_{PE} \frac{\beta_P}{\beta_B} \tag{A2a}$$

and

$$Z_{VP} = r_B h_{BE} \frac{\beta_B}{\beta_P} + r_P h_{PE}, \tag{A2b}$$

where r_B, r_P, h_{BE}, h_{PE} are from Nelson (2001), with slight changes that are described next. Here $r_B = Z_V(2/3\Gamma)^{1/3}/2^{1/2}$ and $r_P = Z_V(2/3\Gamma)^{1/3}\Gamma^{1/2}$ are normalized sizes of the top and bottom (basal) and side (prism) faces, with Γ the column length divided by its diameter. Physically, r_B is the radius of the sphere that would have the same area as the basal faces of the cylinder, scaled by the distance $4D/v$ and written in terms of Z_V for the sphere that would have the same volume. This makes it easier to compare to the spherical case. Similarly, r_P is the scaled radius of the sphere with the same area as the prism faces of the cylinder. The two h functions fit

$$h_{BE}(\Gamma) = \sqrt{2} \cdot 10^{-0.1315\tanh[0.8060\{\log(\Gamma)+0.1854\}-0.0639\log^2(\Gamma)]-0.3314} \tag{A3a}$$

and

$$h_{PE}(\Gamma) = 0.6902 \cdot \Gamma^{-0.5+1/[1.932+0.4976\log(\Gamma)+0.1058\log^2(\Gamma)]}. \tag{A3b}$$

(In Nelson, 2001, the values are half the above, but the product rh is the same). Wood et al. (2001) showed that the above basis functions h are very nearly the same as the corresponding basis functions for a hexagonal column of the same aspect ratio.

Appendix B

Estimated range of x

To estimate x, equate β/β^i to the ratio of surface migration distances (see e.g., Yokoyama and Kuroda, 1990). Measurements of the migration distance of ordinary

ACPD
11, 17423–17445, 2011

water on ice (Mason, Bryant, and van den Huevel, 1963) indicated that it varied rapidly with temperature, decreasing by a factor of five when temperature decreased from −2 to −6 °C, and then increasing again by the same factor from −6 to −12 °C. If the corresponding curve for the isotope on regular ice is similar in shape, but shifted to higher temperature by a degree or more, β/β^i could be as small as 0.2 or as large as 5.0. Such large deviations from unity, however, may be unlikely, so the plots shown here use ratios between 0.8 and 1.2. Such a range is also consistent with measurements of bulk diffusion constants of HDO and $H_2^{18}O$ into ordinary ice given that (a) the migration distance is proportional to the square-root of the diffusion constant and (b) the square-root of the measured ratio of diffusion constants for these two species at 163 K equals 1.3 (Livingston et al, 1997). Although bulk and surface diffusion differ, the measurement shows that two water species can behave differently when diffusing in ice.

Appendix C

Analytic fit for surface impedance

By using a numerical method to solve for Z_S for a range of n, σ_∞/σ_1, and Z_V, and then fitting the curves to an analytic function, I found an approximate formula for β. The formula estimates z within a few percent of the correct value, for the range of possible values of n, σ_∞/σ_1, and Z_V. Specifically, if we use the derived parameter

$$\Phi \equiv \left(\frac{\sigma_\infty}{\sigma_1}\right) Z_V^{\frac{1}{n}}, \tag{C1}$$

then the resulting fitted function is

$$\frac{Z_S}{Z_V} \equiv z(\Phi, n) = 1.5n \frac{\Phi^{-(n/(n+1)-1/4)}}{\log_{10}(1 + 1.5n\Phi^{-(n^2/(n+1)+1/4)})}. \tag{C2}$$

ACPD
11, 17423–17445, 2011

These two equations show that when $\sigma_1 > \sigma_\infty$ and n is large, $z \to (\sigma_\infty/\sigma_1)^{-n} Z_V^{-1}$, which becomes large. In contrast, z decreases as σ_∞ increases. Figure 1 shows both of these trends. Moreover, as Z_V increases during growth, z will decrease during growth.

Appendix D

Symbols used in the text

Symbol	Name	Definition
D	vapor diffusion constant ($m^2\,s^{-1}$)	
d'	vapor diffusion constant ratio	D/D^i
K	hollow volume fraction	hollow volume/total volume
M_j	mass uptake fraction	mass uptake (facet j)/total uptake
M_{NF}	uptake fraction to non-facets	
i	superscript for isotope quantity	
N_{EQ}	vapor density ($\#\,m^{-3}$) at equilibrium	
$N_{S,\infty}$	vapor density at surface, ∞.	
v	gas molecular speed ($m\,s^{-1}$)	
x	deposition coefficient ratio	β/β^i
$x_{B,P}$	x for basal and prism faces	
y	vapor molecular speed ratio	v/v^i
Z	total impedance to growth	Eq. (2)
$Z_{S,V}$	surface, vapor impedance	$1/\beta$, Eq. (A1)
$Z_{VB,VP}$	Z_V for basal, prism faces	Eq. (A2)
z	surface-vapor impedance ratio	Z_S/Z_V
$z_{B,P}$	z for basal, prism faces	

ACPD
11, 17423–17445, 2011

Symbol	Name	Definition
α	fractionation coefficient (‰)	Eq. (6)
$\alpha_{S,KF}$	α for equilibrium, kinetic fractionation	Eqs. (5) and (8)
$\alpha_{B,P}$	α for basal, prism faces	
β	deposition coefficient	Eq. (10)
$\beta_{B,P}$	β for basal, prism faces	
Γ	aspect ratio	crystal length/diameter
γ	growth rate ratio	β_B/β_P
χ	isotope-ordinary water ratio in ice (#/#)	Eq. (4)
σ_S	surface supersaturation	$(N_S - N_{EQ})/N_{EQ}$
σ_∞	supersaturation at ∞	$(N_\infty - N_{EQ})/N_{EQ}$
σ_1, n	parameters for β	Eq. (10)

Acknowledgements. I thank Marcia Baker and Brian Swanson for their critical reading of the manuscript.

References

Burton, W. K., Cabrera, N., and Frank, F. C.: The growth of crystals and the equilibrium structure of their surfaces, Phil. Trans. Royal Soc., London, A243, 299–358, 1951.

Dansgaard, W., Johnsen, S. J., Moller, J., and Langway, Jr., C. C.: One Thousand Centuries of Climatic Record from Camp Century on the Greenland Ice Sheet, Science, 166, 377–380, 1969.

Fisher, D. A.: Remarks on the deuterium excess in precipitation in cold regions, Tellus 43B, 401–407, 1991.

Jouzel, J.: Isotopes in Cloud Physics: Multiphase and Multistage Condensation Processes, Handbook of Environmental Isotope Geochemistry, Vol. 2, The Terrestrial Environment, edited by: Fritz, B. P. and Foutes, J. Ch., Elsevier, 61–112, 1986.

Jouzel, J. and Merlivat, L.: Deuterium and Oxygen 18 in Precipitation: Modeling of the Isotopic Effects During Snow Formation, J. Geophys. Res., 89, 11749–11757, 1984.

ACPD

11, 17423–17445, 2011

Jouzel, J., Alley, R. B., Cuffey, K. M., Dansgaard, W., Grootes, P., Hoffmann, G., Johnsen, S. J., Koster, R. D., Peel, D., Shuman, C. A., Stievenard, M., Stuiver, M., and White, J.: Validity of the temperature reconstruction from water isotopes in ice cores, J. Geophys. Res., 102(C12), 26471–26487, 1997.

Kuroda, T.: Rate Determining Processes of Growth of Ice Crystals from the Vapour Phase, Part I: Theoretical Consideration, J. Meteorol. Soc. Jpn., 62, 552–561, 1984.

Langway Jr., C. C.: The History of Early Polar Ice Cores, ERDC/CRREL TR-08-1, US Army Corps of Engineers, Hanover, NH, 2008.

Lawson, R. P., Baker, B. A., Zmarzly, P., O'Connor, D., Mo, Q., Gayet, J.-F., and Shcherbakov, V.: Microphysical and Optical Properties of Atmospheric Ice Crystals at South Pole Station, J. Appl. Meteor. Clim., 45, 1505–1524, 2006.

Livingston, F. E., Whipple, G. C., and George, S. M.: Diffusion of HDO into Single-Crystal $H_2^{16}O$ Ice Multilayers: Comparison with $H_2^{18}O$, J. Phys. Chem. B, 101, 6127–6131, 1997.

Nelson, J.: Growth mechanisms to explain the primary and secondary habits of snow crystals, Phil. Mag. A, 81, 2337–2373, 2001.

Nelson, J.: Branch Growth and Sidebranching in Snow Crystals, Crystal Growth and Design, 5, 1509–1525, 2005.

Nelson, J. and Baker, M. B.: A New Theoretical Framework for Studies of Vapor Growth and Sublimation of Small Ice Crystals in the Atmosphere, J. Geophys. Res., 101, 7033–7047, 1996.

Mason, B. J., Bryant, G. W., and van den Huevel, A. P.: The growth habits and surface structure of ice crystals, Phil. Mag., 8, 505–526, 1963.

Takahashi, T., Endoh, T., Wakahama, G., and Fukuta, N.: Vapor diffusional growth of free-falling snow crystals between −3 and −23 °C, J. Meteorol. Soc. Jpn., 69, 15–30, 1991.

Uemura, R., Matsui, Y., Yoshida, N., Abe, O., and Mochizuki, S.: Isotopic fractionation of water during snow formation: Experimental evidence of kinetic effect, Polar Meteorol. Glaciol., 19, 1–14, 2005.

Wood, S. E., Baker, M. B., and Calhoun, D.: New model for the vapor growth of hexagonal ice crystals in the atmosphere, J. Geophys. Res., 106(D5), 4845–4870, 2001.

Yokoyama, E. and Kuroda, T.: Pattern formation in growth of snow crystals occurring in the surface kinetic process and the diffusion process, Phys. Rev. A, 41, 2038–2049, 1990.

ACPD
11, 17423–17445, 2011

Table 1. Fractionation factors in Eqs. (8) and (9).

	$1/\alpha_S(0\,^\circ\mathrm{C})$	$1/\alpha_S\ (-20\,^\circ\mathrm{C})$	y^*	d'
$H_2^{18}O$	0.985	0.982	1.054	1.029
HDO	0.883	0.852	1.028	1.025

* Calculated using $v \propto 1/\sqrt{\text{mass}}$.

ACPD
11, 17423–17445, 2011

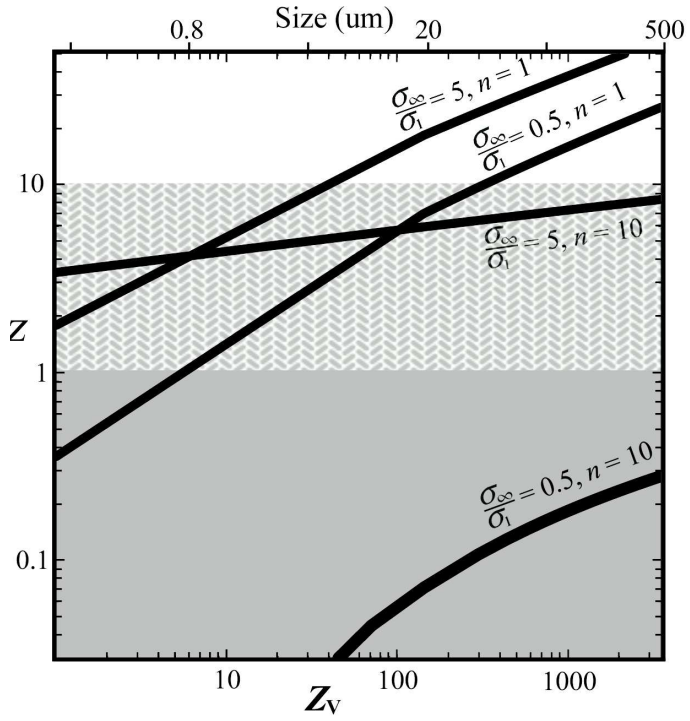

Fig. 1. Relative influence of the surface impedance for a range of vapor impedances (from Eqs. C1 and C2). Each curve represents a crystal with the labeled surface parameters. Crystals in the white zone ($z \geq 10$) likely have fractionation values significantly affected by surface processes, whereas those in the grey zone ($z \leq 1$) will likely not be affected. The case for the hatched region depends on the ratio x. Crystal diameter values on the top scale assume the equation for Z_V of a sphere at 1000 mbar (see Appendix A).

ACPD
11, 17423–17445, 2011

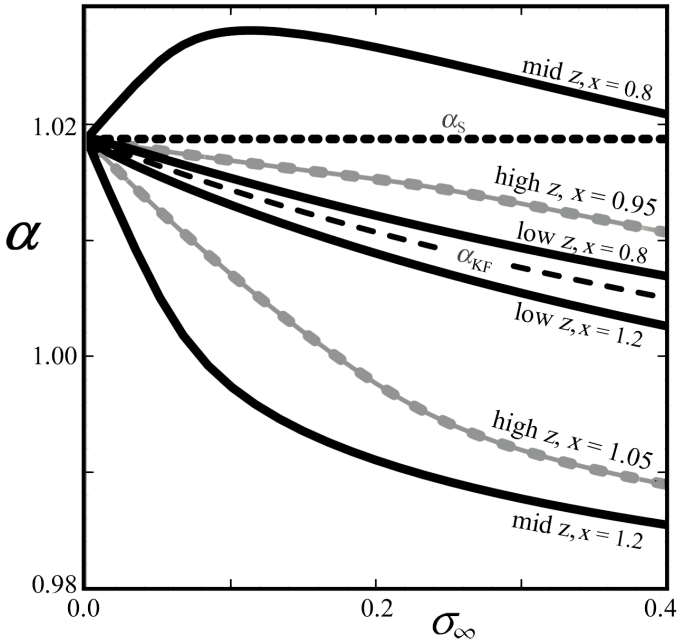

Fig. 2. Calculated $H_2^{18}O$ fractionation coefficients α for ice growing from the vapor at –20 °C and a range of supersaturations σ_∞. Dotted and dashed lines show equilibrium and KF fractionation values. Deviations from the KF prediction depend on $x = \beta/\beta^i$, which is assumed constant, and $z = Z_S/Z_V$, which decreases with increasing σ_∞. Light, beaded curves have the highest z values considered here, exceeding 3.1 at all σ_∞ ($Z_V = 100$, $\sigma_1 = 0.5$, $n = 10$). The two "low z" curves have z values below 0.1 when $\sigma_\infty \geq 0.05$ ($Z_V = 1000$, $\sigma_1 = 0.2$, $n = 1$). The uppermost and lowermost curves have middling z values, exceeding 1 when $\sigma_\infty \leq 0.2$ ($Z_V = 1000$, $\sigma_1 = 0.4$, $n = 5$).

ACPD
11, 17423–17445, 2011

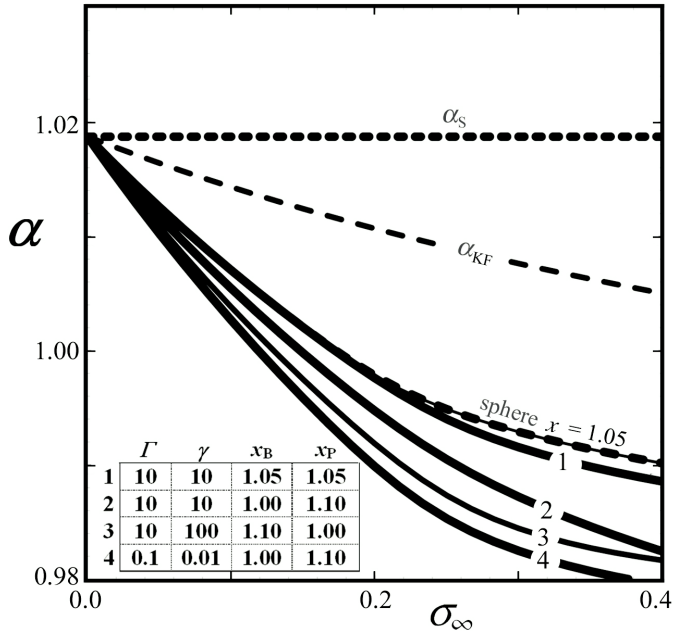

Fig. 3. Fractionation coefficients for cylindrical crystals at $T = -20\,^{\circ}\mathrm{C}$. All cases had the same average x, the same volume ($Z_V = 300$) and growth parameters $\sigma_1 = 0.5$ and $n = 10$ on the fastest-growing face (same as beaded curves in Fig. 2). Cases 1-3 are columnar crystals with $\Gamma = 10$, whereas case 4 is a tabular crystal with $\Gamma = 0.1$. Crystals in cases 1 and 2 grow under steady-state growth, whereas 3 and 4 grow with increasing shape anisotropy.

ACPD
11, 17423–17445, 2011

Theory of isotope fractionation on facetted ice crystals

J. Nelson